Combustion properties of n-heptane/hydrogen mixtures

A. Comandini, Nabiha Chaumeix, J.D. Maclean, G. Ciccarelli

Version of Record: https://www.sciencedirect.com/science/article/pii/S0360319918336425
Manuscript_7c3b7d74543b261e60f67574127b34d3

Combustion properties of n-heptane/hydrogen mixtures

A. Comandini, N. Chaumeix
INSIS, CNRS
Orléans, France

J.D. Maclean, G. Ciccarelli
Department of Mechanical and Materials Engineering, Queen's University
Ontario, Canada

Abstract

The possibility to operate current diesel engines in dual-fuel mode with the addition of hydrogen can be limited by the variation in the combustion properties of the fuel mixture. In the present work, n-heptane was selected as a representative fuel to test the effects of hydrogen addition on the laminar flame speeds and ignition delay times. The spherical bomb technique was used to derive the laminar flame speeds of (n-heptane + hydrogen)/air mixtures (0%, 25%, and 50% hydrogen in the fuel) for an initial temperature of 294 K, pressure of 1 bar, and for equivalence ratios between 0.8 and 1.35. The results showed that average increases of 3% and 10% in the flame speeds were obtained with 25% and 50% hydrogen-enrichment, respectively, while a slight decrease of the Markstein length was obtained. Similar laminar flame speed results were predicted numerically with two kinetic models available in the literature with remarkable accuracy, especially for the Cai and Pitsch model [Cai L, Pitsch H. Combust Flame 2015;162:1623–37]. The kinetic model was subsequently used to perform additional sensitivity and reaction pathway analyses that showed how the chemistry of n-heptane is not substantially influenced by the presence of hydrogen; while the increase in the flame speed is mainly due to the higher concentrations of radical intermediates. The ignition delay times were measured using the reflected shock tube technique for equivalence ratios equal to 0.832, 1.000, and 1.248, initial nominal pressure of 20 bar, temperatures between 730 K and 1200 K, and for different percentages of hydrogen in the fuel (20%, 50%, and 75%). The Cai and Pitsch model once again did a good job of reproducing the experimental data, indicating how at high temperatures the addition of hydrogen does not significantly affect the ignition delay; and in the NTC region (810 K to 920 K) the mixtures composed of (50% n-heptane + 50% hydrogen) and (25% n-heptane + 75% hydrogen) are considerably slower than the reference n-heptane case. This is linked to the concentration of the alkane component and the related low temperature chemistry.

1 Introduction

Current diesel engines use high levels of exhaust gas recirculation to decrease the combustion temperature and minimize the production of NOx. In addition, common rail high pressure fuel injection is used to produce a very fine fuel spray to reduce the production of soot and unburned hydrocarbons. In the latest diesel engines, the use of multiple fuel injections per cycle further reduces the amount of soot. The use of supplemental hydrogen gas mixed with diesel (i.e., hydrogen-enriched diesel) fuel has the potential to decrease these emissions. In fact, the presence of hydrogen reduces the carbon-to-hydrogen ratio and

enhances particle oxidation (producing higher concentrations of H and OH radicals and, for certain operating conditions, higher in-cylinder temperatures). Hydrogen-diesel fuel co-combustion also mitigates the effects of the over-mixing of diesel vapor with air which leads to compositions below the flammability limit and thus to significant concentrations of unburned hydrocarbons leaving the exhaust port. The presence of hydrogen favors flame initiation even in areas of the chamber where the diesel fuel is deficient. On the other hand, the percentage of diesel fuel replaced by hydrogen is limited by abnormal combustion behaviors [1-3]. Since the first pioneering investigations in the eighties [4], numerous diesel-engine studies focused on the effects of hydrogen addition on the exhaust gas composition have been performed. Savaranan and Nagarajan [5] analyzed the emissions from a four-stroke, single-cylinder stationary diesel engine at different brake loads and percentages of hydrogen (between 0% and 90%). The authors measured a reduction in the particulate matter (PM) with increasing amounts of hydrogen (up to about 70% decrease) and in the smoke (caused by poor combustion). In a subsequent study [6], the authors obtained a reduction in the smoke due to particulate matter of around 44% for an optimal hydrogen flow rate of 7.5 lpm. Decrement in PM emissions were also observed by Sandacı and Karagoz [7] (smoke emission values decreased by 57.8%, 70.4%, and 75.2% with 16%, 36%, and 46% hydrogen energy content of total fuel, respectively) similar to other results obtained using the same water cooled, naturally aspirated CFR engine [8] and [9], and by Deb et al. [10] (smoke emission reduced by 37% and 66% with 11% and 42% hydrogen content). Talibi et al. [11] performed experiments on a naturally aspirated, single-cylinder, direct injection, compression-ignition engine fixing the diesel fuel injection period and varying the hydrogen supplied to the engine. A decrease in soot emissions was observed at low engine loads, while at high loads the displacement of intake oxygen by hydrogen is the predominant factor, that leads to a slight increase in PM. A study by Tsolakis et al. [12] showed how the addition of hydrogen to a dual fuel diesel engine operating with reformed exhaust gas recirculation leads to reduced total particle number and mass, but it does not significantly affect particle size and mass distribution. On the other hand, the works by Zhou et al. [13,14] indicate that the decrease in PM emissions is due to the decrease in both particle number and particle size as the hydrogen content increases from 10% to 40%. PM reduction was also obtained by Chaichan [15], although in this case a smaller effect was observed due to the high sulfur content in the diesel fuel. Different considerations apply for the case of the unburned hydrocarbon (HC) emissions. For example, the data obtained by Talibi et al. [11], Savaravnan and Nagarajan [5], and by Köse et al. [16] show a decrease of HC emissions with increasing H_2 enrichment, as in the study by Bari and Esmaeil [17] who evaluated the performance of a conventional diesel engine with addition of O_2/H_2 mixtures. Other studies have shown the contrary [7-10] even if the total HC emissions remain much lower than the regulation limits. In reality, the effect on the HC emissions may depend on the quantity of H_2 introduced, as shown by Zhou et al. [13]. While a consensus has been reached in the case of solid particle emissions, the effect of hydrogen-enriched diesel combustion on NOx is not as clear, since it strongly depends on the operating conditions and the temperatures attained in the combustion chamber. In general, a mild to considerable increase in NOx emissions is expected for increase in the chamber temperature caused by the presence of hydrogen [10,11,14,16]. On the other hand, various studies showed that NOx can be reduced by lowering the combustion temperature at specific operating conditions [5,18–19]. In general, at low loads the NOx emissions decrease with increasing hydrogen content, while the opposite trend is observed at high loads [6,8,13,20]. Moreover, various studies show how for similar loads the addition of small amounts of hydrogen does not modify the NOx emissions while for the case of large H_2 quantities NOx increases considerably [7,9]. Finally, in view of the necessity to reduce fossil fuel consumption, an increase in the thermal engine efficiency was observed in the majority of the above-mentioned studies, due mainly to better mixing between H_2 and air compared to the liquid fuel case and faster burning characteristics (and consequently smaller heat transfer to the walls). Other applications of dual-fuel combustion can be envisioned, for example, in the case of homogeneous charge compression ignition HCCI engines, for which an extensive review has been recently presented by Hairuddin et al. [21]. Several studies have also investigated the combination of hydrogen addition to diesel fuel and exhaust gas recirculation (EGR) techniques to further decrease the engine temperature and consequently the NOx emissions [22-24].

The results obtained for hydrogen-enriched diesel are very promising and emphasize how the technique may have a practical role in reduction of harmful pollutants from transportation engines. To help the engine manufacturers design solutions for an efficient implementation of this technology, the fundamental properties of the hydrogen-enriched diesel fuels need to be investigated not only in engines, but also in research reactors where the chemistry can be easily isolated and studied. In particular, due to the complexity of the real fuels, surrogate mixtures composed of few compounds which mimic the chemical and physical properties of the real fuel are often used in order to simplify CFD engine calculations [25]. In the past, n-heptane has been proposed as a single-component surrogate fuel for diesel [26], and it is the most common component used in multi-component surrogate formulations, including the widely used primary reference fuel PRF and toluene reference fuel TRF. Due to its importance, n-heptane chemistry has been studied in detail both experimentally and numerically, in particular regarding its combustion properties, i.e. ignition delay times and laminar flame speeds, as relevant to the functioning of modern combustion devices. Several shock tube studies on n-heptane/air mixtures were implemented for the measurement of ignition delay times over a wide range of temperatures (720-1400 K), pressures (2-60 atm), and stoichiometric conditions (ϕ between 0.1 and 3) [27-33]. These studies were extended to lower temperature conditions (600-960 K) using rapid compression machine measurements at stoichiometric and fuel lean conditions and pressures between 3 and 20 atm [34-39]. Other ignition delay time measurements with shock tube devices were also performed in argon bath gas for dilution factors between 64% and 99%, pressures between 1 and 15 atm, fuel-lean, and for stoichiometric and fuel-rich conditions [40-48]. In addition, regarding the laminar flame speed, n-heptane has been extensively studied in the literature by means of various experimental techniques, including Bunsen burners, horizontal tubes, counterflow flames, spherical bombs, stagnation jets, and heat flux burners [49-63]. Considering the latest, more reliable datasets, the experimental results cover a wide range of pressures (0.5-25 atm), temperatures (298-470 K), and equivalence ratios (0.6-1.7). The objective of this study is to experimentally analyze the effects of hydrogen addition to the fundamental combustion properties of n-heptane using well-characterized kinetic experimental apparatuses. Aggarwal [64] used chemical kinetic model simulation to study the ignition of n-heptane/H_2 and n-heptane/CH_4 mixtures. On the other hand, to the best of our knowledge, this work provides for the first time data which will be essential to validate chemical kinetic models for use in dual-fuel engine design codes. Kinetic analyses will also be performed based on kinetic models available in the literature.

2 Experimental and modeling techniques

Spherical reactor facility

The technique has been presented in detail in previous publications [65–66]. The spherical reactor is a stainless steel vessel composed of two concentric spheres with optical access guaranteed by the presence of 4 quartz windows (100 mm optical diameter). The diameter of the internal sphere is around 47.5 cm, which results in a volume of 56 liters. The gaseous mixtures of interest are prepared directly inside the vessel using the partial pressure method. Two MKS Baratron capacitive manometers (Type 631) of different full scales (100 Torr and 1000 Torr) are connected directly to the bomb for measurement of the partial pressures of the fuel and the air according to the required pressure ranges. The use of the two manometers minimizes the maximum error in the mixture preparation, estimated to be 0.5% for the single measurements and thus 1% for the equivalence ratios. The vacuum limit of the reactor is around 10^{-2} Torr and the gases left in the reactor are mainly composed of N_2, H_2O, and CO_2. The effect of the residual gases is then minimal. In the present work three different experimental datasets were obtained with 0%, 25%, and 50% of hydrogen in n-heptane. The composition of the air is 0.209 O_2 + 0.791 N_2 (laboratory dry air), while the purities of n-heptane and hydrogen were 99.8% (Sigma-Aldrich) and 99.999% (Alphagaz 1, Air Liquide), respectively. The high quality of the fuels reduces the risk of contaminations. All the experimental results were obtained at an initial pressure and temperature of 100 kPa and 294±1 K, respectively.

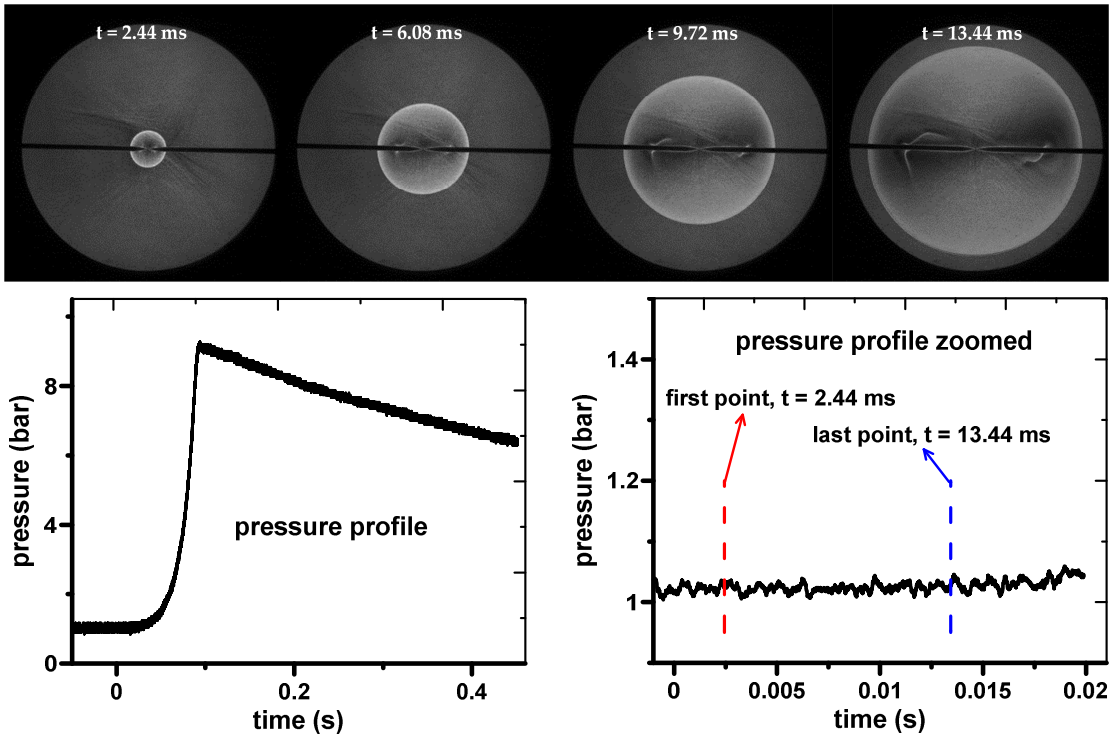

Figure 1. (50% n-heptane + 50% H_2) / air flame, stoichiometric conditions.

After the mixture preparation inside the reactor, the flame is initiated at the center of the sphere by a spark obtained with two tungsten electrodes located on the same diameter of the sphere but of course in opposite directions. The distance between the tips of the two electrodes was adjusted in order to obtain, for each equivalence ratio, flames which were spherical and unperturbed by the presence of the electrodes. The spherical bomb is coupled to a Z-type single-pass schlieren system for visualization of the flame, a high-speed camera (Phantom v1610) with fixed frame rate of 25000 fps for image recording, and a Kistler pressure transducer (Kistler 601A) for monitoring of the pressure during the combustion process. Figure 1 shows the stoichiometric (50% n-heptane + 50% H_2) / air flame as a function of time. As mentioned above, the flame propagates starting from the center of the sphere till it reaches the limit of the window, which is also the last point which can be used for measuring the flame propagation speed. It is important to notice how the flame is spherical along the entire observation window while its surface is only slightly disturbed by the electrodes. The separation between the burned and the fresh gases is easily identifiable. These characteristics are essential in order to obtain accurate measurements of the radii and to guarantee the validity of the fundamental assumptions on which the expanding flame theory is based. The different signals are synchronized, thus the pressure rise due to the gas expansion can be directly correlated with the flame propagation. As shown in Figure 1, the combustion in closed vessels leads to a large increase of the pressure (in the present case, the maximum pressure is around 7 bar at 0.1 seconds). On the other hand, the pressure over a much shorter time (between 2.44 and 13.44 ms in the specific case) is nearly constant (graph at the bottom-right of Figure 1). In particular, the pressure rise between the times of the first and the last images used for deriving the flame speed is between 0.5% and 0.9% in the present experiments, thus it is accurate to assume that the flame propagates at nearly constant pressure conditions. This is possible because the volume of the burned gases which corresponds to the diameter of the windows is much smaller than the total volume of the sphere (around 0.8%).

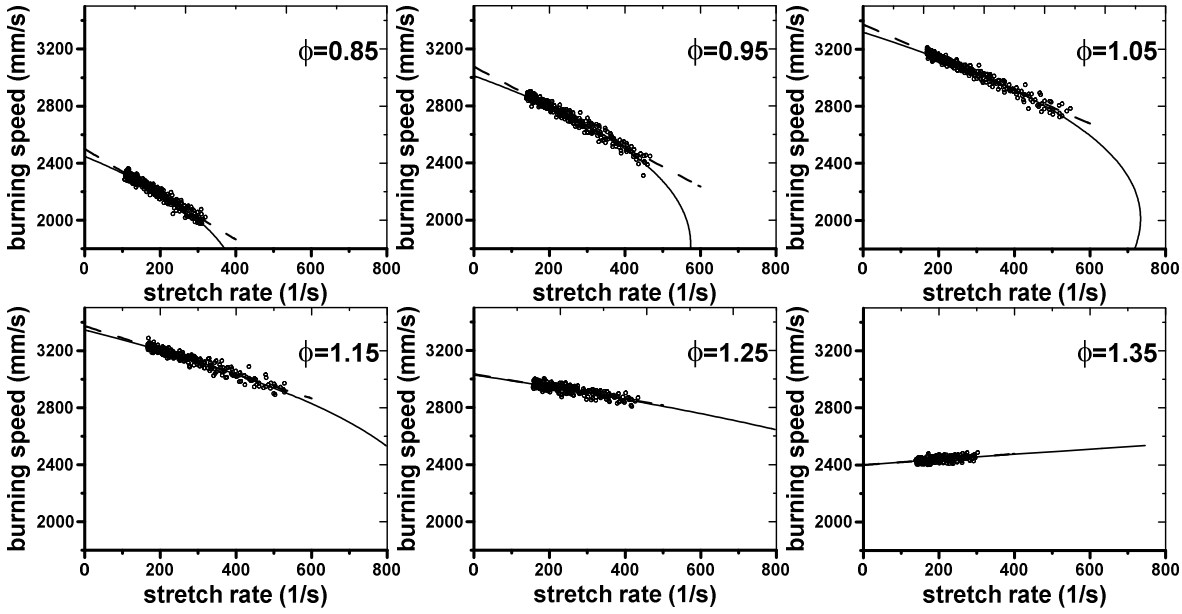

Figure 2. Laminar burning speed, (50% n-heptane + 50% H2) / air. Solid line: NQ model; dash line: LS model.

The use of automated Matlab software based on the Canny method allowed the derivation of the flame radius as a function of time starting from the flame images. The stretched laminar flame speed of the burned gases is subsequently derived from the radii. For obtaining the unstreatched laminar flame speed of the burned gases relative to the flame speed, S_b^0, and the Markstein length, L_b, the following expression proposed by Ronney and Sivashinsky [67] and by Kelley and Law [68] was solved:

$$\left(\frac{S_b}{S_b^0}\right)^2 \cdot \ln\left(\frac{S_b}{S_b^0}\right)^2 = -\frac{2L_b \cdot \kappa}{S_b^0} \qquad (1)$$

where κ is the stretch rate. Finally, the fundamental value of the unstretched laminar flame speed of the unburned gases, S_u^0, was derived using the simple continuity equation which for the case of constant pressure conditions simplifies to $S_u^0 = S_b^0/\sigma$. In this equation the value of sigma is defined as $\sigma = \rho_u/\rho_b$ where ρ_u and ρ_b are the unburned and burned gas densitiesas calculated using COSILAB [69]. Based on the uncertainties in the radii (± 1 pixel), an error of around ±0.6 cm/s in the flame speed measurements was estimated.

The measured unstretched spatial laminar burning speed obtained using the non-linear method (NQ) corresponding to eq. 1 is shown in Figure 2 for different equivalence ratios. The scales of the x- and y-axes are identical for all the graphs. This allows a direct visual comparison between the different cases, not only in terms of unstretched flame speed (defined as the intersection between the fitting curve and the y-axis) but also in terms of experimental trends. The slope of the fitting curve is directly related to the Markstein length, which clearly decreases with increasing equivalence ratios (L_b is even negative valued for ϕ = 1.35). Also shown in Figure 2 is the linear relation between burning speed and stretch rate ($S_b = S_b^0 - L_b \cdot \kappa$, [70–71], denoted as LS). The two solutions are very similar at fuel rich conditions, while they differ for the fuel lean cases. This is due to the fact that the linear model is not able to correctly

reproduce the speed vs stretch relation for the entire range of equivalence ratios studied herein. Other extrapolation methods proposed in the literature [72-74] were also tested in order to confirm the accuracy of the present extrapolation methodology and estimate the associated uncertainties. The solutions of the NM-I model by Chen [72] (solid line) and the non-linear model in expansion form NE [73] (dash line) are presented in Figure 3 together with the NQ solution (circles). The maximum discrepancy between the results obtained with the NM-I and NE methods (which are almost superimposed) compared to the results derived from the NQ equation (symbols) is around 1.3%, which is well within the uncertainties of the measurements. Thus, the extrapolation model does not have an influence on the derivation of the laminar flame speeds. Wu et al. [74] proposed a different criterion in order to discriminate the spherical expanding flame experiments which may be affected by large errors due to the extrapolation method. Based on such criterion, the product between the Markstein number and the Karlovitz number (Ma·Ka) must be below 0.15 for reliable measurements. This is the case for all the experiments presented here (Figure 4). It is important to underline how such a criterion was developed based on experimental databases for hydrogen and n-heptane fuels. The results presented in Figure 4 can be then considered without any doubt as a valid confirmation of the accuracy of the extrapolation method. Finally, the iterative procedure used to solve equation 1 was also tested. Chen [72] proposed a different formulation of equation 1 (NM-II) which can be solved with a least-square method. The two mathematical approaches give very similar solutions.

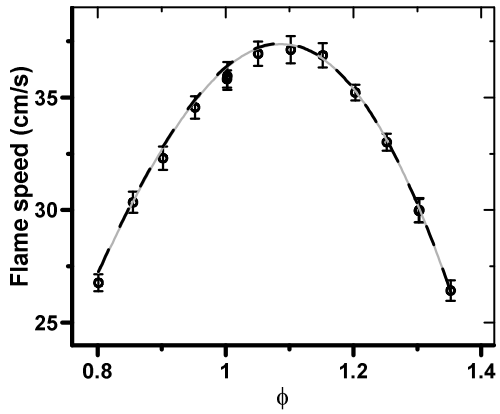

Figure 3. Laminar flame speed measurements obtained with different extrapolation methods for n-heptane/air measurements. Symbols: NQ, —— NM-I, – – NE.

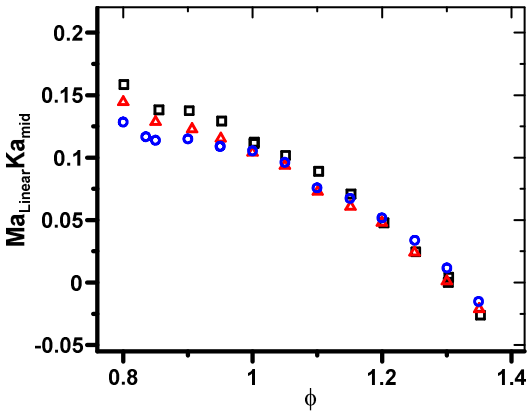

Figure 4. Criterion to estimate the extrapolation error by Wu et al. [74]: $Ma_{Linear} \cdot Ka_{mid}$. Negligible error for $-0.05 < Ma_{Linear} \cdot Ka_{mid} < 0.15$. □ 100% C_7H_{16}, △ 75% C_7H_{16} + 25% H_2, ○ 50% C_7H_{16} + 50% H_2.

Another physical aspect which may cause uncertainties in the measurement of the laminar flame speed is the heat radiation from the burned to the unburned gases. The simplified model by Yu et al. [75] provides a simple tool to estimate the effects of radiation on the experimental measurements from expanding flames. Based on this approach, the radiation-correction terms are around 0.5 cm/s for all the experimental conditions. If the corrections were applied to all the experimental points, a simple shift of the profiles by 0.5 cm/s would be obtained. Such a shift would not modify the effect of the hydrogen addition on the laminar flame speeds.

Shock Tube Facility

The shock tube has a 4.5 m long, 7.6 cm square cross-section driven-section and a 1.83 m long, 10.2 cm diameter driver. A 76.2 cm round-to-square transition section is included in the driven length. The double diaphragm technique was used to accurately obtain the desired shock Mach number. The diaphragm material is 2 mm thick, 1100 series aluminum, pressed with a four-petal shape to facilitate diaphragm opening (rupture pressure between 22.1 and 44.2 bar across the diaphragms). Three piezoelectric pressure transducers (PCB 113A24) are used to record the pressure inside the tube and consequently to obtain the incident shock wave velocity. The distance between successive pressure transducers is 0.31 m, with the last one located at the axial position of the reflection endplate. The incident shock wave velocities were subsequently used together with the initial conditions to calculate the pressure and temperature conditions behind the reflected shock waves by solving the conservation equations. The method used for the calculations assumes thermal equilibrium, no reaction before ignition, and variable specific heat ratio. Based on the dimension of the pressure transducer face there is a possible error of 1.74% on the shock speed, and therefore, the maximum estimated errors in the temperature and pressure conditions behind the reflected shock waves are 2.5% and 5.8%, respectively. A photodiode (Edmund Optics, S-050-H) with a 430±10 nm filter (Thorlabs, FB430-10) is attached to the endplate via an acrylic rod to detect luminescence from CH radicals. The onset of ignition was determined by the maximum slope in the pressure profiles, which also corresponds to a steep increase in the CH radical signals measured by the photodiode. Ignition delay times have been defined as the time between the arrival of the incident shock wave at the end plate and the onset of ignition. A typical pressure profile is presented in Figure 5, also shown is the ignition delay time. The shock tube is pumped down using an Edwards RV5 pump (designed vacuum of 2×10^{-3} mbar). The fuel/air mixtures were prepared in a separate mixing chamber using the method of partial pressures to combine n-heptane, hydrogen and air at the desired ratios. In the present study, the percentage of hydrogen in the fuel mixture was varied from 0% to 20%, 50%, and 75%, for average equivalence ratios equal to 1.248, 1.000, and 0.832.

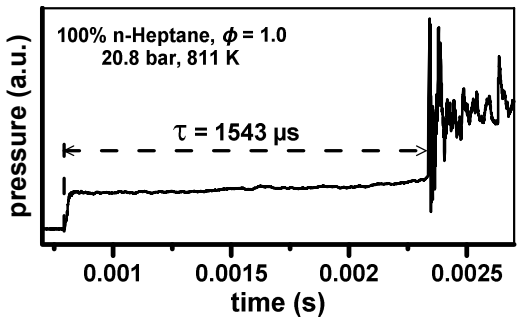

Figure 5. Typical pressure profile; n-heptane/air mixture, $\phi = 1$, $T_5 = 811$ K, $P_5 = 20.8$ bar.

Chemical kinetic modeling

As mentioned in the previous sections, n-heptane has been the focus of numerous studies including the development and validation of detailed chemical kinetic models. Various models have nowadays reached excellent performances with respect to the simulation of both the ignition delay times and the laminar flame speeds of n-heptane/air mixtures, such as for example the LLNL model [76] (654 species and 2827 reactions), the NUIG model [77] (1268 species and 5336 reactions), or the CRECK model [78] (300 species and 11790 reactions, including chemistry for iso-octane). These models are relatively large in terms of number of species and reactions which makes them impractical for use in engine codes. Even for simulations of laminar flame speed measurements the resulting computational costs are considerable. For these reasons, reduction schemes have been developed to diminish the size of the models based on specific targets. In view of their practical use in engine simulations and their reduced computational costs, two reduced chemical kinetic schemes were used in the present work to simulate the laminar flame, these include the models by Stagni et al. [79] and Cai and Pitsch [80]. The two models provide very similar results compared to the non-reduced models, with-respect-to laminar flame speed measurements of gasoline PFR/toluene surrogates, including experimental results for the n-heptane component available in the literature. The iso-octane chemistry was removed by both models, which reduced their size to 236 species and 1165 reactions for the model by Cai and Pitsch [80] and 106 species and 791 reactions for the model by Stagni et al. [79]. The present work includes the addition of hydrogen as a fuel, thus the corresponding C0 reactions were analyzed in detail. In particular, the model by Stagni et al. [79] does not contain the recombination reactions between two hydrogen atoms and two oxygen atoms as in the original CRECK model [81, 82], thus, these reactions were added. The addition of such reactions did not change the simulation results for the n-heptane experiments. The validation of the two models against experimental hydrogen/air data at room temperature and atmospheric pressure from the literature is presented in Figure 6. The two models generate very similar results, in good agreement with the experimental data over the entire range of equivalence ratios, thus they can be used with confidence to model the hydrogen enriched n-heptane experiments. Cosilab software, version 3.3.2 [69] was used to perform the simulations. In particular, the one-dimensional freely-propagating flames were solved to derive the laminar flame speed. GRAD and CURV were imposed as 10^{-5}, with a spatial domain between -10 and 100 mm, while multi-component transport properties and Soret effect were included in the calculations. The model by Cai and Pitsch [80] was also used to simulate the ignition delay time together with the CRECK model [82]. In this case, the simulations were obtained with the homogeneous batch reactor module at adiabatic, constant volume conditions and at an initial pressure of 20 bar.

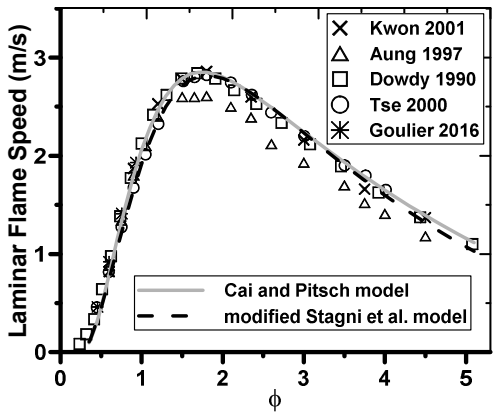

Figure 6. Laminar flame speed of H_2/air. T_{in} = 298 K; P_{in} = 101.3 kPa: × Kwon et al. [83], △ Aung et al. [84], □ Dowdy et al. [85], ○ Tse et al. [86], ✳ Goulier et al. [87].

3 Results and discussions

Numerous studies on laminar flame speed of n-heptane/air mixtures provide a benchmark to confirm the validity of the spherical bomb technique. The n-heptane/air measurements were compared to the measurements at room temperature and atmospheric pressure available in the literature (see Figure 7). Also provided in Figure 7 is the normalized data taking into account the difference in initial temperature (294 K vs 298 K), pressure (100 kPa vs 101.3 kPa), and air composition. The normalization factors were estimated using the kinetic model by Cai and Pitsch [80]: all the simulations were performed first at the conditions of the present study, then at the conditions of the data in the literature, from which normalization factors could be derived. Figure 7 clearly shows that the present data closely agree with the recent measurements by Dirrenberger et al. [63] obtained with a flat flame adiabatic burner.

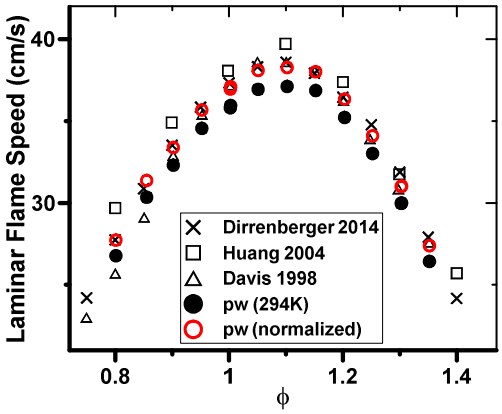

Figure 7. Laminar flame speed of n-heptane/air. T_{in} = 298 K; P_{in} = 101.3 kPa: × Dirrenberger et al. [63], □ Huang et al. [54], △ Davis et al. [52]. ● present work (T_{in} = 294 K; P_{in} = 100 kPa); ○ p.w. normalized to 298 K (see text)

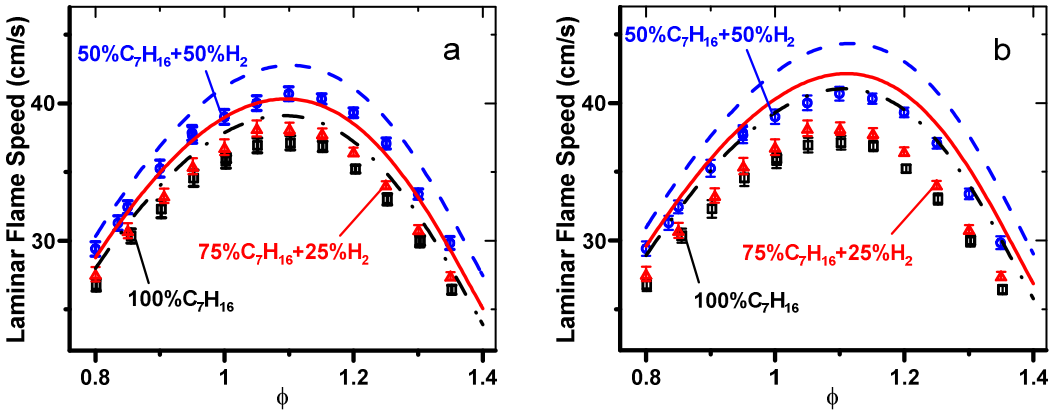

Figure 8. Laminar flame speed of n-heptane/H_2/air mixtures. Fuels: □ 100% C_7H_{16}, △ 75% C_7H_{16} + 25% H_2, ○ 50% C_7H_{16} + 50% H_2. Lines represent modeling results using the model by: a) Cai and Pitsch [80], Stagni et al. [79].

The experimentally measured laminar flame speeds are reported in Figure 8, together with the simulations obtained with the two kinetic models. The blending of hydrogen with n-heptane leads to an incremental change in the laminar flame speed. The term "speed increment" is used to represent the difference between the laminar flame speed for the hydrogen/heptane and the heptane-only fuel. The change is substantial only when a large amount of hydrogen is present. Figure 9 contains the experimental

and modeling increments obtained for different hydrogen enrichment. The experimental flame speed data was fit with a polynomial, see Figure 8. The fits accurately reproduce the experimental results, with discrepancies which are within the experimental error of a single measurement (less than 0.3 cm/s for more than 90% of the cases). The results in Figure 9 indicate that the addition of 25% of hydrogen in the fuel mixture generates an average increase of only 3% in the speed (0.9 cm/s on average, with maximum increment of ~ 1.2 cm/s at $\phi \sim 1.1$). On the other hand, the laminar flame speeds of the (50% C_7H_{16} + 50% H_2)/air mixtures are ~10% higher than the n-heptane case (3.3 cm/s on average). In this case, the maximum increment is reached at $\phi \sim 1.2$, thus slightly shifted compared to the experiments with lower hydrogen mole fractions. From a modeling perspective, both models overpredict the measurements (Figure 8), although the error can be considered minimal (around 5% for the Cai and Pitsch model [80] and between 6% and 14% for the Stagni et al. model [79], with higher discrepancies at fuel-rich conditions). A more important aspect evident in Figure 9 is that both models are capable to reproduce quite accurately the effects of the addition of H_2. In particular, the correspondence between the results obtained with the Cai and Pitsch model [80] (dash lines) and the experiments is remarkable for both profiles. The only discrepancy appears at fuel-rich conditions, where the experimental profiles bend at lower equivalence ratios and thus the speed increments are slightly over-predicted.

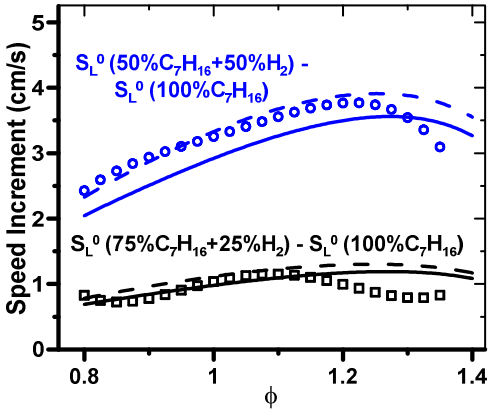

Figure 9. Increment of the flame speed for different hydrogen enrichment compared to the n-heptane/air case. Dashed lines: Cai and Pitsch model [80]; solid lines: Stagni et al. model [79].

The effect of hydrogen addition on the experimental Markstein length (derived from the solution of the non-linear equation) was also considered. The Markstein length L is related to the slope of the curves in Figure 2: the higher the slope, the larger the corresponding value of L. Figure 10a shows the renormalized burned Markstein length L′ (L′ = L_b/σ). This value is consistent with the plots of the unstretched laminar flame speed of the unburned gases. Considering the curves which fit the experimental data, the addition of hydrogen slightly decreases the Markstein length at fuel-lean conditions, 6-8% and 16-18% for the (75% C_7H_{16} + 25% H_2) and (50% C_7H_{16} + 50% H_2) datasets compared to pure n-heptane, respectively. As an example, three different curves obtained at $\phi \sim 0.95$ are presented in Figure 10b. Even if the extrapolated flame speed is lower for the case of n-heptane (black line and symbols), the slope of the corresponding curve is clearly larger than the curves obtained with hydrogen enrichment. Although the estimated error in the determination of L′ is larger than the observed differences, the small discrepancy between the polynomial fits and the experimental data suggests that the error estimates on the single measurements may be conservative, larger than the actual values. Thus, hydrogen enrichment is expected to slightly change the response of the flame to the stretch as in engine applications (for fuel-lean conditions). Finally, for fuel-rich conditions the curves presented in Figure 10a converge, suggesting no effect of the hydrogen enrichment on the response of the flame to stretch.

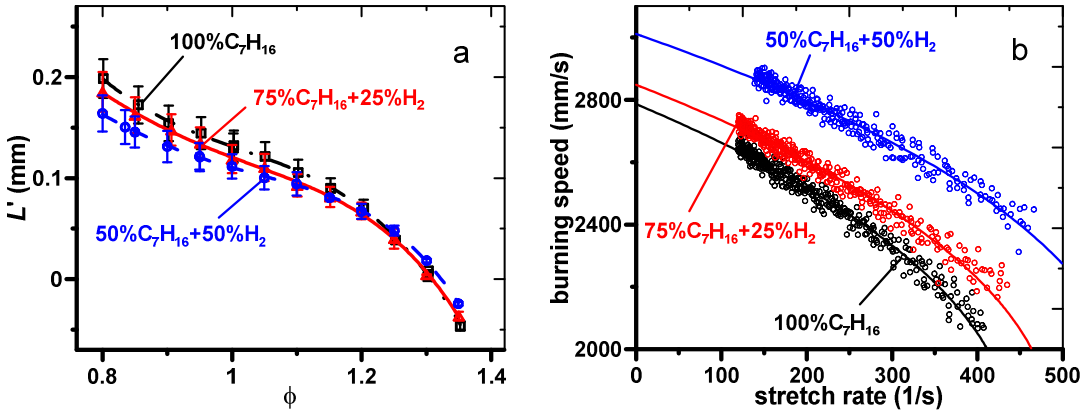

Figure 10. a) Markstein length L′; b) evolution of the spatial laminar burning speed, $\phi \sim 0.95$.

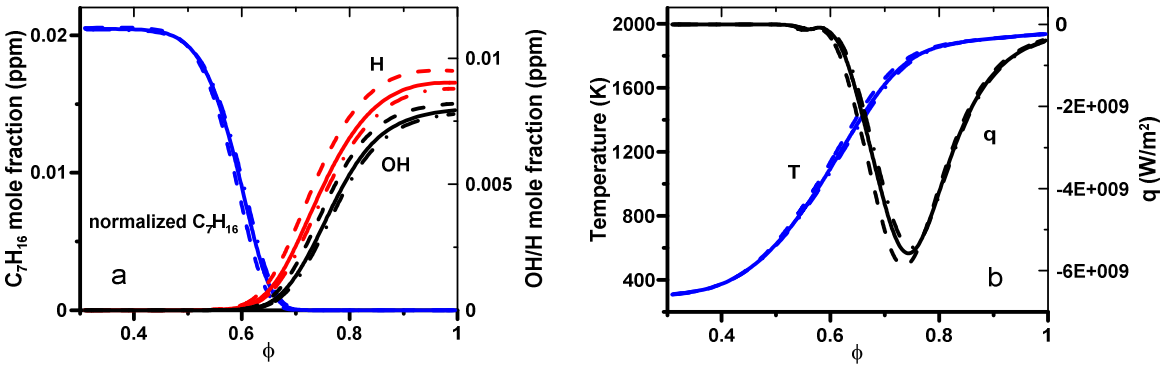

Figure 11. Profiles for a) normalized C_7H_{16} (blue); OH (black), H (red); b) temperature (blue), heat release rate (black). $\phi = 1.1$. Dash-dot line (100% C_7H_{16}); solid line (75% C_7H_{16} + 25% H_2), dash line (50% C_7H_{16} + 50% H_2).

The chemical kinetic models were also used to determine how the fuel composition influences flame propagation. The results presented in the following paragraphs were obtained with the kinetic Cai and Pitsch model [80], which provides better predictions of the measured laminar flame speed. The main factor which leads to the increase in the flame speed with increased percentages of hydrogen enrichment is the formation of larger amounts of radicals (in particular H, OH, and HO_2). The H and OH profiles are reported in Figure 11a for $\phi = 1.1$. The addition of 25% hydrogen in the fuel leads to an increase of 2.8% and 1.7% in the maximum H and OH mole fractions, respectively; while for (50% C_7H_{16} + 50% H_2) the maxima increased by 8.2% and 2.7%. The radicals diffuse towards the unburned gas leading to faster consumption of the n-heptane (as shown in Figure 11a, where the profiles were normalized based on the fuel mole fraction of the 100% C_7H_{16} case) and a larger heat release rate (Figure 11b). In this case, the increase in the peak heat release rate is 2.5% and 8.2% for 25% and 50% hydrogen enrichment, respectively. These results agree with measurements made in IC engines [5]. Although the adiabatic flame temperature changes only slightly (2272K, 2274 K, and 2277 K for 0%, 25%, and 50% hydrogen at stoichiometric conditions), the temperature profiles follow the same behavior of the fuel and the heat release rate; thus a steeper slope for higher hydrogen enrichment is observed in Figure 11b. From a practical point-of-view, the absolute mole fraction of the radicals, as presented in Figure 11a, determine the variation in the flame propagation speed in engines (for similar equivalence ratios), but such values are influenced by the different initial mole fractions of H atoms. The H atom profiles relative to the H atom content in the 100% C_7H_{16} case are reported in Figure S1 (Supplementary File). The difference in H atom

concentration peaks becomes less marked than in Figure 11a, but the addition of hydrogen leads to an increase in the production of H atoms relative to the initial H content in the fuel. This suggests that the chemistry of hydrogen is more effective in producing H atoms compared to the n-heptane chemistry, which is of course an expected result.

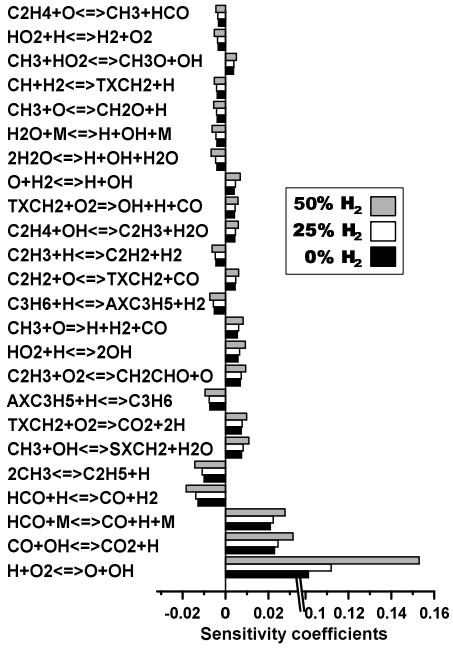

Figure 12. Sensitivity analysis of the laminar flame speed with respect to the reaction rate constants, $\phi = 1.1$.

Although some of the pathways for the n-heptane consumption are more-or-less favored by the presence of hydrogen, the reactions which significantly affect the flame propagation speed remain unaltered. Figure 12 shows the sensitivity analysis of the laminar flame speed with respect to the reaction rate constants for $\phi = 1.1$. All the coefficients increase when hydrogen is added to the fuel mixture, which is mainly due to presence of larger radical mole fractions (as shown in Figure 11a). On the other hand, the reaction order remains nearly identical. This is due to two facts: 1) the flame speed is mainly influenced by the H_2/O_2 chemistry and by the small intermediates produced from the decomposition of n-heptane; 2) there is not a substantial variation in the pathways which leads to the formation of such small fragments. Such pathways are presented in Figure 13, for reactions leading to propene, allyl radical, ethylene, ethyl radical, and acetylene, intermediates whose chemistry significantly affects the flame propagation speed. The purpose of this figure is not to provide a comprehensive description of the n-heptane chemistry, but to show the effects of the presence of hydrogen on the decomposition of regular carbon-based fuels, in this case n-C_7H_{16}. The arrow thickness is proportional to the integrated reaction rates for the n-heptane/air mixture, while the numbers represent the percentage increase/decrease for the (50% C_7H_{16} + 50% H_2) fuel mixture compared to the pure n-heptane case (after normalization to take into account the number of C atoms in the fuels). For clarity, the figure has been divided into two parts, where the formation pathways for the compounds highlighted by dash lines (bottom graph) are reported on the upper graph. It is clear how hydrogen increases the rate of consumption of the fuel (as already observed concerning Figure 11), and consequently of the intermediates due to the increase in H, OH, and HO_2 concentrations. Only the fluxes proceeding through the thermal decomposition of the largest stable olefins (such as 1-hexene (C_6H_{12}) and 1-pentene (C_5H_{10}) forming C_3H_5 + C_3H_7 and C_3H_5 + C_2H_5 respectively) drop due to the considerable increase in the competing H-abstraction reactions by H, OH, and O radicals. Similarly, the

fragmentation of the resonantly stabilized allyl radical to acetylene + methyl radical shows a decrease of 11.2% due to competition with reactions involving the H atoms (recombination to form propene and addition/fragmentation to form C_2H_3 + CH_3).

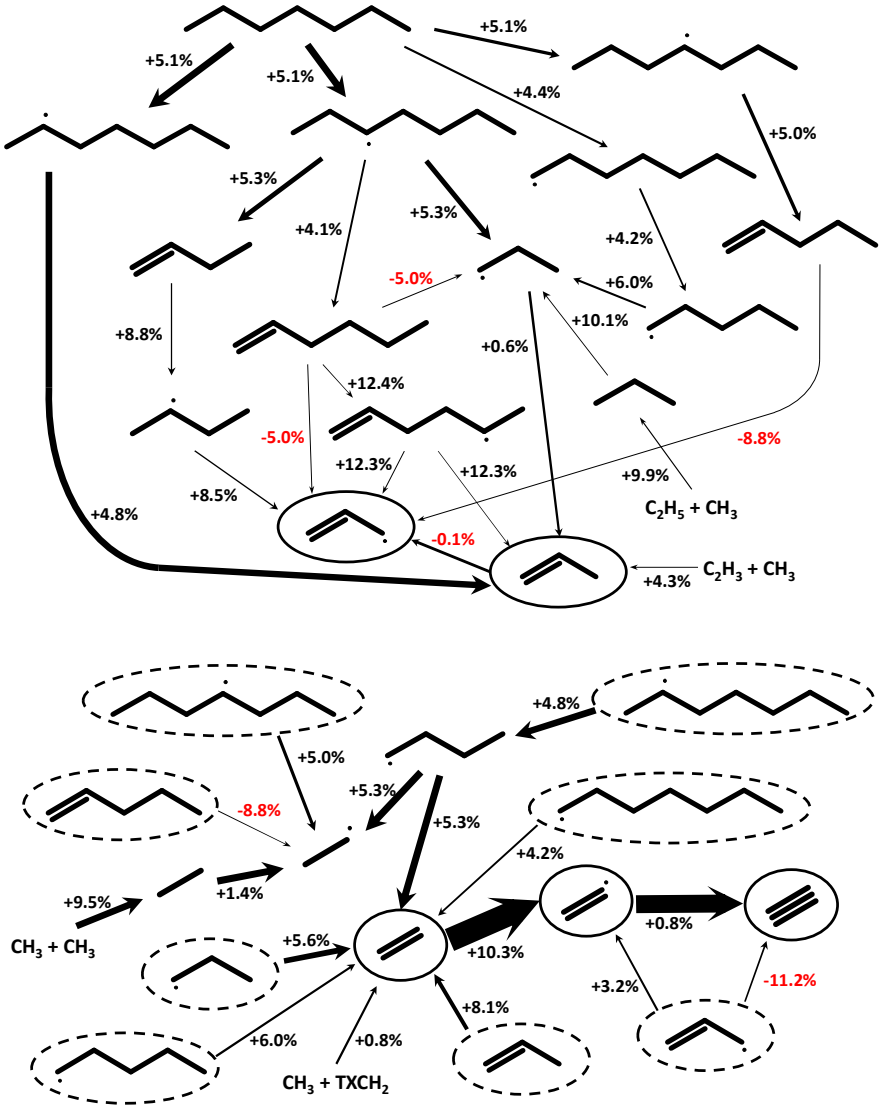

Figure 13. Rate of consumption analysis, ϕ = 1.10. Arrow thickness proportional to the integrated reaction rates for C_7H_{16}/air mixture. Percentages represent the increment/decrement for the (50% C_7H_{16} + 50% H_2) fuel mixture compared to the pure n-heptane (after normalization to take into account the number of C atoms in the fuels). Dash lines for compounds whose formation is reported on the upper graph.

As for the case of the laminar flame speed, various studies on the ignition delay times of n-heptane/air mixtures have been completed in the past. The experiments presented herein were obtained at a nominal initial pressure of 20 bar, varying the equivalence ratio between 0.832 and 1.248. The comparison between the stoichiometric results and the ones available in the literature for similar pressure conditions by Ciezki and Adomeit [27] and Gauthier et al. [30] are reported in Figure 14a. The experiments are in good agreement over the entire temperature range (730 K - 1200 K), especially in the negative temperature

coefficient (NTC) region between 810 K and 920 K, where the ignition time increases with increasing temperature. In the rest of the study, attention is focused on NTC region which corresponds to the post compression operating temperature in typical IC engines. The measured ignition delay time for n-heptane/air for equivalence ratios between 730 K and 950 K is presented in Figure 14b. In general, there is slight decrease in the ignition delay for an increase in equivalence ratio from 0.832 to 1.0, but almost no change from 1.0 to 1.248. A similar trend was observed for different hydrogen enrichments.

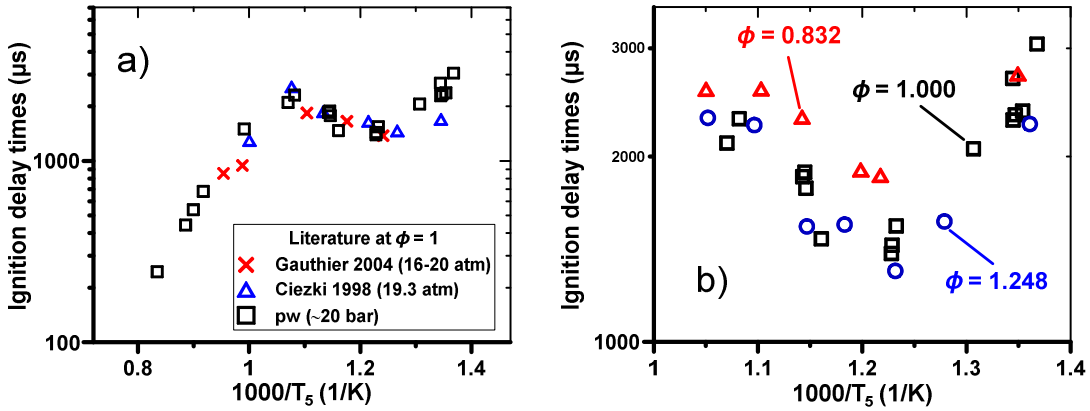

Figure 14. Ignition delay times of n-heptane/air mixtures. a) Comparison of stoichiometric mixtures with the literature: □ present work; △ Ciezki and Adomeit [27]; × Gauthier et al. [30]; b) NTC region results (present work): □ ϕ = 1.000; △ ϕ = 1.248; ○ ϕ = 0.832.

The experimental and modeling results for different hydrogen enrichment are presented in Figure 15. From the experiments, no discernable difference could be observed between the different datasets in the high temperature region, while in the NTC region the experimental data differs more significantly. In particular, the ignition delay times of (80% n-heptane + 20% hydrogen)/air mixtures nearly superimpose for pure n-heptane, and only with higher hydrogen enrichment does the ignition delay time increase (as was the case of the laminar flame speed). Similar results were obtained with the two kinetic models which are capable of reproducing, not only the effects of hydrogen addition, but also the magnitude of the experimental data. The Cai and Pitsch model [80] accurately predicts the experimental results over the entire temperature range, especially in the NTC region, while the increase in the ignition delay time in the NTC region is slightly overpredicted by the CRECK model [82].

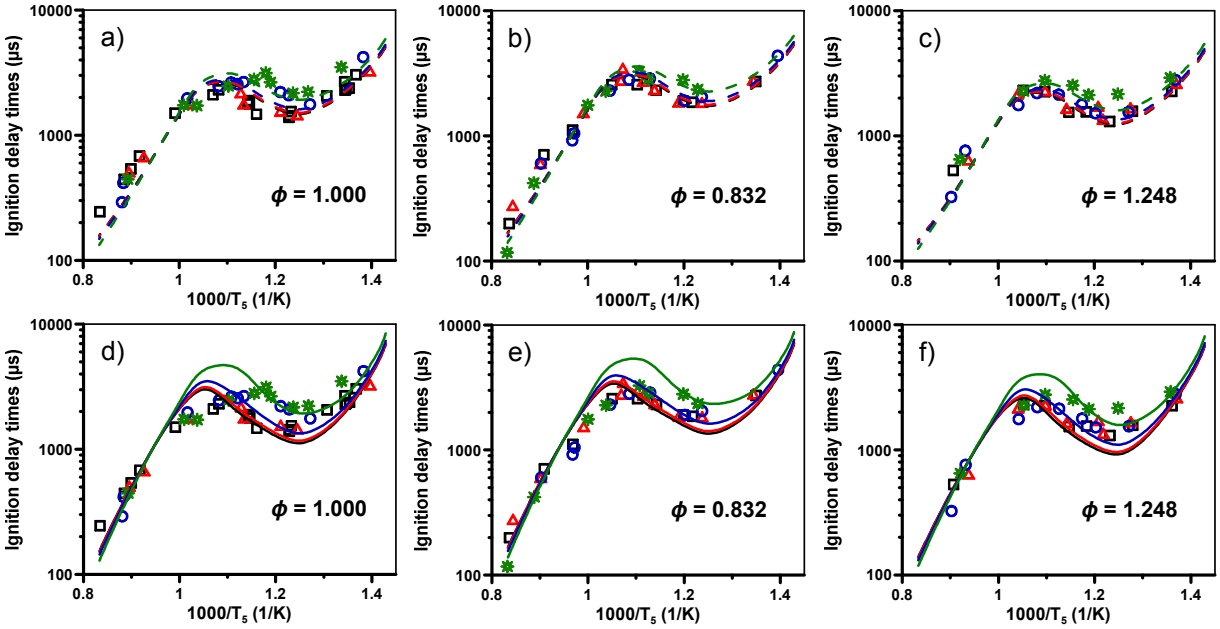

Figure 15. Ignition delay times of n-heptane/H_2/air mixtures for 3 different equivalent ratios and nominal pressures of 20 bar: a) & d) ϕ = 1.000, b) & e) ϕ = 0.832, c) & f) ϕ = 1.248. Fuels: □ 100% C_7H_{16}, △ 80% C_7H_{16} + 20% H_2, ○ 50% C_7H_{16} + 50% H_2, ✲ 25% C_7H_{16} + 75% H_2. Dashed lines: Cai and Pitsch model [80]; solid lines: CRECK [82].

	20% H_2	**50% H_2**	**75% H_2**
T = 900 K	2.2%	9.1%	29.9%
T = 850 K	2.0%	8.4%	27.4%
T = 800 K	1.9%	7.8%	25.7%
T = 750 K	1.7%	7.2%	23.6%

Table 1. Average calculated increase in ignition delay time for different hydrogen enrichment compared to the C_7H_{16}/air reference case.

Since the uncertainty in the experimental results does not allow to accurately determine the effects of hydrogen enrichment on the ignition delay time (many more points would be necessary in order to draw reliable fitting curves), the model by Cai and Pitsch which better fits the experimental curves was used for this purpose. The percentage increase in the ignition delay time for different hydrogen enrichment compared to the reference n-heptane/air is reported in Table 1 for temperatures between 750 K and 900 K (temperature range relevant to diesel engines). The data indicated is the average of the values for the three equivalence ratios investigated. In all cases, the effects of the hydrogen addition are slightly more marked at higher temperatures, although the mixtures composed of 80% n-heptane and 20% hydrogen are characterized by ignition delay times which differ by only ~ 2% compared to the reference case. The percentage increase becomes larger with increased hydrogen enrichment, ~ 8% and ~ 27% for (50% C_7H_{16} + 50% H_2) and (25% C_7H_{16} + 75% H_2), respectively. These variations are mainly due to the drop in the concentration of the n-heptane and oxygen components in the initial mixture. For example, the n-heptane mole fraction at stoichiometric conditions diminishes by 1.6%, 6.0%, and 16% with the addition of 20%, 50%, and 75% of hydrogen, respectively. Therefore, the low temperature chemistry becomes less significant, as shown in Figure 16b where the mole fractions of the most abundant peroxy radical (3-hepthyl peroxy, $C_7H_{15}O_2$) are present. The higher the concentration of initial hydrogen, the lower the mole fraction of the intermediate species formed through the low temperature kinetic mechanisms. This

translates to a smaller increase in pressure and temperature conditions due to cool flame phenomenon (see Figure 16a), which directly affects the ignition delay times, i.e., the lower the temperatures reached due to the cool flame, the longer the delay.

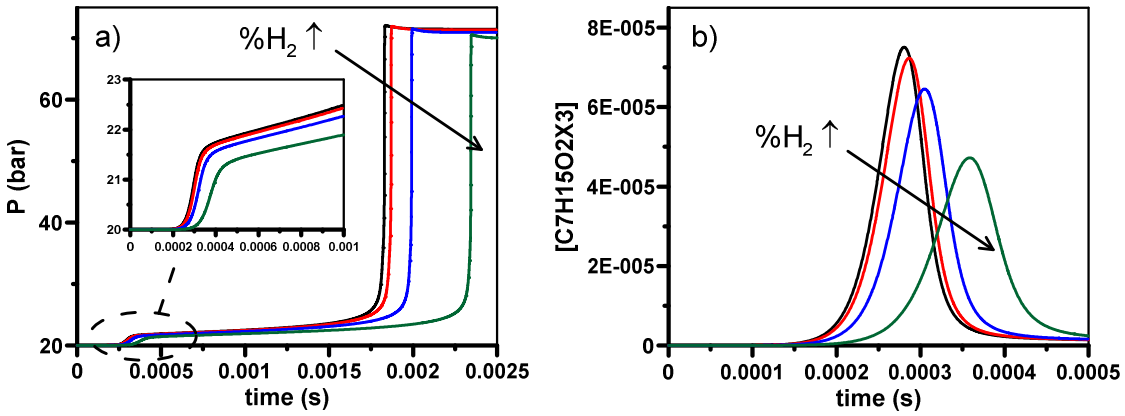

Figure 16. a) Pressure and b) 3-heptyl peroxy profiles predicted by the Cai and Pitsch model [80] for $\phi = 1$ at an initial temperature of 850 K.

4 Conclusions

The effect of hydrogen enrichment on the combustion properties of n-heptane/air has been investigated both experimentally, using complementary techniques, and numerically with kinetic models available in the literature. New laminar flame speed measurements in n-heptane/air, (75% n-heptane + 25% hydrogen)/air, and (50% n-heptane + 50% hydrogen)/air mixtures were obtained at an initial pressure of 1 bar and initial temperature of 294 K. The results show that the flame speed increases by roughly 3 % and 10 % with 25% and 5% hydrogen enrichment of n-heptane, accompanied by a slight decrease in the Markstein length. The experiments on the ignition delay times of fuel/air mixtures containing from 0% to 75% hydrogen enrichment were conducted at equivalence ratios of 0.832, 1.000, and 1.248, initial nominal pressures of 20 bar, with particular focus on the NTC region which is relevant to diesel engine post compression conditions. Only for large hydrogen enrichment does the ignition delay time become longer compared to the reference n-heptane/air case. The simulations accurately reproduce the experimentally measured laminar flame speed and the ignition delay time. The kinetics behind the change in the combustion properties of the n-heptane/hydrogen dual fuel were identified. From a practical point-of-view, the control of the ignition delay time and the heat release rate could be accomplished by adjustments in the operational parameters for optimal dual-fuel engine performance (for similar equivalence ratios).

Acknowledgments

The authors would like to thank Kevin Brialix for the support in running the laminar flame speed experiments. The work was partially financed by the Centre Nationnal de la Recherche Scientifique and Natural Sciences and Engineering Research Council of Canada.

References

[1] Szwaja S, Grab-Rogalinski K. Hydrogen combustion in a compression ignition diesel engine. Int J Hydrogen Energy 2009;34:4413–4421.

[2] Tsujimura T, Suzuki Y. The utilization of hydrogen in hydrogen/diesel dual fuel engine. Int J Hydrogen Energy 2017;42:14019–14029.

[3] Liew C, Li H, Nuszkowski J, Liu S, Gatts T, Atkinson R, Clark, N. An experimental investigation of the combustion process of a heavy-duty diesel engine enriched with H2. Int J Hydrogen Energy 2010;35:11357–11365.

[4] Gopal G, Srinivasa Rao P, Gopalakrishnan KV, Murthy BS. Use of hydrogen in dual-fuel engines. Int J Hydrogen Energy 1982;7:267–272.

[5] Saravanan N, Nagarajan G. An experimental investigation of hydrogen–enriched air induction in a diesel engine system. Int J Hydrogen Energy 2008;33:1769–1775.

[6] Saravanan, N.; Nagarajan, G. Performance and emission studies on port injection of hydrogen with varied flow rates with Diesel as an ignition source. Applied Energy 87;7:2218–2229.

[7] Sandalci T, Karagöz Y. Experimental investigation of the combustion characteristics, emissions and performance of hydrogen port fuel injection in a diesel engine. Int J Hydrogen Energy 2014;39:18480–18489.

[8] Karagöz Y, Sandalci T, Yüksek L, Dalkiliç AS. Engine performance and emission effects of diesel burns enriched by hydrogen on different engine loads. Int J Hydrogen Energy 2015;40:6702–6713.

[9] Karagöz Y, Güler I, Sandalci T, Yüksek L, Dalkiliç AS. Effect of hydrogen enrichment on combustion characteristics, emissions and performance of a diesel engine. Int J Hydrogen Energy 2016;41:656–665.

[10] Deb M, Sastry GRK, Bose PK, Banerjee R. An experimental study on combustion, performance and emission analysis of a single cylinder, 4-stroke DI-diesel engine using hydrogen in dual fuel mode of operation. Int J Hydrogen Energy 2015;40:8586–8598.

[11] Talibi M, Hellier P, Balachandran R, Ladommatos N. Effect of hydrogen–diesel fuel co–combustion on exhaust emissions with verification using an in–cylinder gas sampling technique. Int J Hydrogen Energy 2014;39:15088–15102.

[12] Tsolakis A, Hernandez JJ, Megaritis A, Crampton M. Dual Fuel Diesel Engine Operation Using H2. Effect on Particulate Emissions. Energy Fuels 2005;19:418–425.

[13] Zhou JH, Cheung CS, Leung CW. Combustion, performance, regulated and unregulated emissions of a diesel engine with hydrogen addition. Applied Energy 2014;126:1–12.

[14] Zhou JH, Cheung, CS, Zhao WZ, Leung CW. Diesel-hydrogen dual-fuel combustion and its impact on unregulated gaseous emissions and particulate emissions under different engine loads and engine speeds. Energy 2016;94:110–123.

[15] Chaichan MT. The Effects of Hydrogen Addition to Diesel Fuel on the Emitted Particulate Matters. Int J Sci Eng Res 2015;6:1081–1087.

[16] Köse H, Ciniviz M. An experimental investigation of effect on diesel engine performance and exhaust emissions of addition at dual fuel mode of hydrogen. Fuel Process. Technol. 2013;114:26–34.

[17] Bari S, Mohammad Esmaeil M. Effect of H2/O2 addition in increasing the thermal efficiency of a diesel engine. Fuel 2010;89:378–383.

[18] Masood M, Ishrat MM. Computer simulation of hydrogen–diesel dual fuel exhaust gas emissions with experimental verification. Fuel 2008;87:1372–1378.

[19] Christodoulou F, Megaritis A. Experimental investigation of the effects of simultaneous hydrogen and nitrogen addition on the emissions and combustion of a diesel engine. Int J Hydrogen Energy 2014;39:2692–2702.

[20] Saravanan N, Nagarajan G, Sanjay G, Dhanasekaran C, Kalaiselvan KM. Combustion analysis on a DI diesel engine with hydrogen in dual fuel mode. Fuel 2008;87:3591–3599.

[21] Hairuddin AA, Yusaf T, Wandel AP. A review of hydrogen and natural gas addition in diesel HCCI engines. Renew Sust Energ Rev 2014;32:739–761.

[22] Banerjee R, Roy S, Bose PK. Hydrogen-EGR synergy as a promising pathway to meet the PM-NOx-BSFC trade-off contingencies of the diesel engine: A comprehensive review. Int J Hydrogen Energy 2015;40:12824–12847.

[23] Bose PK, Maji D. An experimental investigation on engine performance and emissions of a single cylinder diesel engine using hydrogen as inducted fuel and diesel as injected fuel with exhaust gas recirculation. Int J Hydrogen Energy 2009;34:4847–4854.

[24] Miyamoto T, Hasegawa H, Mikami M, Kojima N, Kabashima H, Urata Y. Effect of hydrogen addition to intake gas on combustion and exhaust emission characteristics of a diesel engine. Int J Hydrogen Energy 2011;36:13138–13149.

[25] Pitz WJ, Mueller CJ. Recent progress in the development of diesel surrogate fuels. Progr Energy Combust Sci 2011;37:330–350.

[26] Guo H, Neill WS, Chippior W, Li H, Taylor JD. An Experimental and Modeling Study of HCCI Combustion Using n-Heptane. J Eng Gas Turb Power 2009;132:022801.

[27] Ciezki HK, Adomeit G. Shock-tube investigation of self-ignition of n-heptane-air mixtures under engine relevant conditions. Combust Flame 1993;93:421–433.

[28] Fieweger K, Blumenthal R, Adomeit G. Shock-tube investigations on the self-ignition of hydrocarbon-air mixtures at high pressures. Proc Combust Inst 1994;25:1579–1585.

[29] Fieweger K, Blumenthal R, Adomeit G. Self-ignition of S.I. engine model fuels: A shock tube investigation at high pressure. Combust Flame 1997;109:599–619.

[30] Gauthier BM, Davidson DF, Hanson RK. Shock tube determination of ignition delay times in full-blend and surrogate fuel mixtures. Combust Flame 2004;139:300–311.

[31] Herzler J, Jerig L, Roth P. Shock tube study of the ignition of lean n-heptane/air mixtures at intermediate temperatures and high pressures. Proc Combust Inst 2005;30:1147–1153.

[32] Shen H-PS, Steinberg J, Vanderover J, Oehlschlaeger MA. A Shock Tube Study of the Ignition of n-Heptane, n-Decane, n-Dodecane, and n-Tetradecane at Elevated Pressures. Energy Fuels 2009;23:2482–2489.

[33] Hartmann M, Tian K, Hofrath C, Fikri M, Schubert A, Schießl R, Starke R, Atakan B, Schulz C, Maas U, Kleine Jäger F, Kühling K. Experiments and modeling of ignition delay times, flame structure and intermediate species of EHN-doped stoichiometric n-heptane/air combustion. Proc Combust Inst 2009;32:197–204.

[34] Minetti R, Carlier M, Ribaucour M, Therssen E, Sochet LR. A rapid compression machine investigation of oxidation and auto-ignition of n-Heptane: Measurements and modeling. Combust Flame 1995;102:298–309.

[35] Karwat DMA, Wagnon SW, Wooldridge MS, Westbrook CK. Low-temperature speciation and chemical kinetic studies of n-heptane. Combust Flame 2013;160:2693–2706.

[36] Cox A, Griffiths JF, Mohamed C, Curran HJ, Pit WJ, Westbrook CK. Extents of alkane combustion during rapid compression leading to single-and two-stage ignition. Proc Combust Inst 1996;26:2685–2692.

[37] Griffiths JF, Halford-Maw PA, Mohamed C. Spontaneous ignition delays as a diagnostic of the propensity of alkanes to cause engine knock. Combust Flame 1997;111:327–337.

[38] Tanaka S, Ayala F, Keck JC, Heywood JB. Two-stage ignition in HCCI combustion and HCCI control by fuels and additives. Combust Flame 2003;132:219–239.

[39] Silke EJ, Curran HJ, Simmie JM. The influence of fuel structure on combustion as demonstrated by the isomers of heptane: a rapid compression machine study. Proc Combust Inst 2005;30:2639–2647.

[40] Vasu SS, Davidson DF, Hanson RK. OH time-histories during oxidation of n-heptane and methylcyclohexane at high pressures and temperatures. Combust Flame 2009;156:736–749.

[41] Vermeer DJ, Meyer JW, Oppenheim AK. Auto-ignition of hydrocarbons behind reflected shock waves. Combust Flame 1972;18:327–336.

[42] Coats CM, Williams A. Investigation of the ignition and combustion of n-heptane-oxygen mixtures. Proc Combust Inst 1979;17:611–621.

[43] Burcat AF, Richard F.; Matula, Richard A. Shock Initiated Ignition in Heptane-Oxygen-Argon Mixtures. 13th Int Symp on Shock Tubes and Waves 1981;826–833.

[44] Colket MB, Spadaccini LJ. Scramjet Fuels Autoignition Study. J Propul Power 2001;17:315–323.

[45] Horning DC, Davidson DF, Hanson RK. Study of the High-Temperature Autoignition of n-Alkane/O/Ar Mixtures. J Propul Power 2002;18:363–371.

[46] Imbert B, Catoire L, Chaumeix N, Paillard C. Ignition Delays of Heptane/O2/Ar Mixtures in the 1300-1600 K Temperature Range. J Propul Power 2004;20:415–426.

[47] Smith JM, Simmie JM, Curran HJ. Autoignition of heptanes; experiments and modeling. Int J Chem Kinet 2005;37:728–736.

[48] Akih-Kumgeh B, Bergthorson JM. Comparative Study of Methyl Butanoate and n-Heptane High Temperature Autoignition. Energy Fuels 2013;24:2439–2448.

[49] Gerstein M, Levine O, Wong EL. Flame Propagation. II. The Determination of Fundamental Burning Velocities of Hydrocarbons by a Revised Tube Method. J Am Chem Soc 1951;73:418–422.

[50] Heimel S, Weast RC. Effect of initial mixture temperature on the burning velocity of benzene-air, n-heptane-air, and isooctane-air mixtures. Proc Combust Inst 1957;6:296–302.

[51] Gibbs GJ, Calcote HF. Effect of Molecular Structure on Burning Velocity. J Chem Eng Data 1959;4:226–237.

[52] Davis SG, Law CK. Laminar flame speeds and oxidation kinetics of iso-octane-air and n-heptane-air flames. Proc Combust Inst 1998;27:521–527.

[53] Kwon OC, Hassan MI, Faeth GM. Flame/Stretch Interactions of Premixed Fuel-Vapor/O/N Flames. J Propul Power 2000;16:513–522.

[54] Huang Y, Sung CJ, Eng JA. Laminar flame speeds of primary reference fuels and reformer gas mixtures. Combust Flame 2004;139:239–251.

[55] Kumar K, Freeh JE, Sung CJ, Huang Y. Laminar Flame Speeds of Preheated iso-Octane/O2/N2 and n-Heptane/O2/N2 Mixtures. J Propul Power 2007;23:428–436.

[56] Smallbone AJ, Liu W, Law CK, You XQ, Wang H. Experimental and modeling study of laminar flame speed and non-premixed counterflow ignition of n-heptane. Proc Combust Inst 2009;32:1245–1252.

[57] Jerzembeck S, Peters N, Pepiot-Desjardins P, Pitsch H. Laminar burning velocities at high pressure for primary reference fuels and gasoline: Experimental and numerical investigation. Combust Flame 2009;156:292–301.

[58] Ji C, Dames E, Wang YL, Wang H, Egolfopoulos FN. Propagation and extinction of premixed C5-C12 n-alkane flames. Combust Flame 2010;157:277–287.

[59] Chong CT, Hochgreb S. Measurements of laminar flame speeds of liquid fuels: Jet-A1, diesel, palm methyl esters and blends using particle imaging velocimetry (PIV). Proc Combust Inst 2011;33:979–986.

[60] Kelley AP, Smallbone AJ, Zhu DL, Law CK. Laminar flame speeds of C5 to C8 n-alkanes at elevated pressures: Experimental determination, fuel similarity, and stretch sensitivity. Proc Combust Inst 2011;33:963–970.

[61] van Lipzig JPJ, Nilsson EJK, de Goey LPH, Konnov AA. Laminar burning velocities of n-heptane, iso-octane, ethanol and their binary and tertiary mixtures. Fuel 2011;90:2773–2781.

[62] Sileghem L, Alekseev VA, Vancoillie J, Van Geem KM, Nilsson EJK, Verhelst S, Konnov AA. Laminar burning velocity of gasoline and the gasoline surrogate components iso-octane, n-heptane and toluene. Fuel 2013;112:355–365.

[63] Dirrenberger P, Glaude PA, Bounaceur R, Le Gall H, da Cruz AP, Konnov AA, Battin-Leclerc F. Laminar burning velocity of gasolines with addition of ethanol. Fuel 2014;115:162–169.

[64] Aggarwal SK, Awomolo O, Akber K. Ignition characteristics of heptane-hydrogen and heptane-methane fuel blends at elevated pressures. Int J Hydrogen Energy 2011;36:15392–15402.

[65] Nativel D, Pelucchi M, Frassoldati A, Comandini A, Cuoci A, Ranzi E, Chaumeix N, Faravelli T. Laminar flame speeds of pentanol isomers: An experimental and modeling study. Combust Flame 2016;166:1–18.

[66] Comandini A, Pengloan G, Abid, S, Chaumeix, N. Experimental and modeling study of styrene oxidation in spherical reactor and shock tube. Combust Flame 2016;173:425–440.

[67] Ronney P, Sivashinsky G. A Theoretical Study of Propagation and Extinction of Nonsteady Spherical Flame Fronts. SIAM Journal on Applied Mathematics 1989;49:1029–1046.

[68] Kelley AP, Law CK. Nonlinear effects in the extraction of laminar flame speeds from expanding spherical flames. Combust Flame 2009;156:1844–1851.

[69] COSILAB. The Combustion Simulation Laboratory, Version 3.3.2. http://www.SoftPredict.com. Rotexo GmbH & Co. KG, Haan, Germany, 2009.

[70] Clavin P. Dynamic behaviour of premixed flame fronts in laminar and turbulent flows. Progr Energy Comb Sci 1985;11:1–59.

[71] Matalon M, Matkowsky BJ. Flames as gasdynamic discontinuities. J Fluid Mech 1982;124:239–259.

[72] Chen Z. On the extraction of laminar flame speed and Markstein length from outwardly propagating spherical flames. Combust Flame 2011;158:291–300.

[73] Kelley AP, Bechtold JK, Law CK. J Fluid Mech 2011691:26–51.

[74] Wu F, Liang W, Chen Z, Ju Y, Law CK. Uncertainty in stretch extrapolation of laminar flame speed from expanding spherical flames. Proc Combust Inst 2015;35:663–670.

[75] Yu H, Han W, Santner J, Gou X, Sohn CH, Ju Y, Chen Z. Radiation–induced uncertainty in laminar flame speed measured from propagating spherical flames. Combust Flame 2014;161:2815–2824.

[76] Mehl M, Pitz WJ, Westbrook CK, Curran HJ. Kinetic Modeling of Gasoline Surrogate Components and Mixtures Under Engine Conditions, Proc Combust Inst 2011;33:193–200.

[77] Zhang K, Banyon C, Bugler J, Curran HJ, Rodriguez A, Herbinet O, Battin-Leclerc F, B'Chir C, Heufer KA. An updated experimental and kinetic modeling study of n-heptane oxidation. Combust Flame 2016;172:116–135.

[78] Pelucchi M, Bissoli M, Cavallotti C, Cuoci A, Faravelli T, Frassoldati A, Ranzi E, Stagni A. Improved Kinetic Model of the Low-Temperature Oxidation of n-Heptane. Energy Fuels 2014;28:7178–7193.

[79] Stagni A, Frassoldati A, Cuoci A, Faravelli T, Ranzi E. Skeletal mechanism reduction through species–targeted sensitivity analysis. Combust Flame 2016;163:382–393.

[80] Cai L, Pitsch H. Optimized chemical mechanism for combustion of gasoline surrogate fuels. Combust Flame 2015;162:1623–1637.

[81] Frassoldati A, Faravelli T, Ranzi E. A wide range modeling study of formation and nitrogen chemistry in hydrogen combustion. Int J Hydrogen Energy 2006;31:2310–2328.

[82] Ranzi E, Frassoldati A, Grana R, Cuoci A, Faravelli T, Kelley AP, Law CK. Hierarchical and comparative kinetic modeling of laminar flame speeds of hydrocarbon and oxygenated fuels. Prog. Energy Combust. Sci. 2012;38;468–501.

[83] Kwon OC, Faeth GM. Flame/stretch interactions of premixed hydrogen–fueled flames: measurements and predictions. Combust Flame 2001;124:590–610.

[84] Aung KT, Hassan MI, Faeth GM. Flame stretch interactions of laminar premixed hydrogen/air flames at normal temperature and pressure. Combust Flame 1997;109:1–24.

[85] Dowdy DR, Smith DB, Taylor SC, Williams A. The use of expanding spherical flames to determine burning velocities and stretch effects in hydrogen/air mixtures. Proc Combust Inst 1991;23:325–32.

[86] Tse SD, Zhu DL, Law CK. Morphology and burning rates of expanding spherical flames in H2/O2/inert mixtures up to 60 atmospheres. Proc Combust Inst 2000;28:1793–800.

[87] Goulier J, Comandini A, Halter F, Chaumeix N. Experimental study on turbulent expanding flames of lean hydrogen/air mixtures. Proc Combust Inst 2017;36:2823–2832.